Urban Climate 49 (2023) 101544

Contents lists available at ScienceDirect

Urban Climate

journal homepage: www.elsevier.com/locate/uclim

Associations between summer wind environment and urban physical indicators in commercial blocks based on field measurement and simulation in Xi'an

Qian Zhang [a,b,*], Rui Dong [c], Duo Xu [d], Dian Zhou [a,d], Alessandro Rogora [b]

[a] Technology Innovation Center for Land Engineering and Human Settlements, Shaanxi Land Engineering Construction Group Co.,Ltd and Xi'an Jiaotong University, China
[b] Department of Architecture and Urban Studies, Politecnico di Milano, Piazza Leonardo da Vinci, Milano 26, 20133, Italy
[c] CCCC First Highway Consultants CO.LTD., No.62 Keji 2nd Road, Xi'an, Shaanxi Province, China
[d] School of Human Settlements and Civil Engineering, Xi'an Jiaotong University, No.99 Yanxiang Road, Xi'an, Shaanxi Province, China

ARTICLE INFO

Keywords:
Wind environment
Commercial block
Spatial morphology
Xi'an

ABSTRACT

As a major driving force to improve economic output, commercial blocks also play a significant role in enhancing urban vitality. Due to its characteristics of high building density and large building volume, many wind environment problems are likely to appear in commercial blocks. In this research, we simulated the wind environment of four theoretical block models and real commercial blocks in STREAM software. The results suggest that under the same other conditions, the wind speed inside the block is the lowest when its building footprint ratio reaches about 56%. When the building footprint ratio is greater than 56.3% and gradually increasing, or less than 39.1% and gradually decreasing, the wind speed both inside and around the block will be steadily increased. In addition, we also found the quantitative correlations between the wind environment and other urban physical indicators, such as mean building height, stagger ratio of building height and enclosure degree, according to which we proposed the adjustment strategies of the spatial form of commercial blocks. Finally, we used four cases to verify the effectiveness of these strategies in optimizing the wind environment of commercial blocks.

1. Introduction

1.1. Background

To accommodate the increasing urban population, global cities are expanding rapidly, and the construction intensity is rising steadily. The expansion of cities not only provides convenience for human beings, but also makes us fall into some unprecedented crises. Such as air pollution, urban heat wave, urban heat island and some other environmental problems, all of which are related to the reduction of urban natural ventilation. Studies have shown that optimizing urban wind environment can effectively improve various urban microclimate problems. However, urban wind climate becomes more fragile with the disorder of urban spatial layout (Hallegatte and Corfee-Morlot, 2010). Hence, how to optimize the urban wind environment by adjusting block spatial forms is the main

* Corresponding author at: Department of Architecture and Urban Studies, Politecnico di Milano, Piazza Leonardo da Vinci, Milano 26, 20133, Italy.
E-mail address: qian.zhang@polimi.it (Q. Zhang).

https://doi.org/10.1016/j.uclim.2023.101544
Received 4 May 2022; Received in revised form 14 March 2023; Accepted 19 April 2023
Available online 24 April 2023

problem discussed in this study.

In the past decade, some new types of commercial space have appeared in China due to changes in the types of commercial activities. Their location and spatial layout have a great impact on the urban spatial structure. Current design of commercial blocks focuses more on functions and economic benefits, and rarely considers environmental factors. However, a neglected fact is that the microclimate quality of commercial space has a great influence on its attractiveness and commercial value. It should be regarded as an important design indicator. The research on urban microclimate involves many different disciplines, including environment, climate, urban planning and architectural design (Golany, 1996). Contemporary research has confirmed a correlation between various indicators of urban spatial forms and wind environments from multiple perspectives (Du et al., 2022; Palusci et al., 2022). However, a detailed quantitative analysis is still lacking to comprehend the effects of different urban spatial forms on wind environments.

1.2. Current research

At present, the research on the wind environment at block scale is mainly about the street canyon. It refers to the part bounded by streets and buildings on both sides. (Oke, 1988) took the lead in conducting preliminary research on wind environment of street canyon. Later, many scholars have carried out numerical simulations based on his research conclusions to explore the relationship between street height width ratio and wind environment (Dirksen et al., 2019; Elshaer et al., 2017; B.-J. He et al., 2014; A. Zhang et al., 2005).

After calculating dozens of street canyon models, (Shashua-Bar and Hoffman, 2004) found the impact of urban spatial indicators such as street height width ratio and building depth on urban microclimate. A joint research team composed of scholars from the United States, Denmark and Britain analyzed the influence of the roof configuration on wind environment of street canyon by using turbulence models (Kastner-Klein et al., 2004). By analyzing the climate data measured in the field investigation, (Georgakis and Santamouris, 2006) summarized the variation laws of wind environment and thermal environment in street canyon. By simulating the planting patterns of various street trees, (Yang et al., 2018) studied the influence of vegetation morphology on the microclimate of street canyon.

In addition to the research on the wind environment of street canyon, many scholars have studied the correlation between various urban spatial indicators and wind environment in the past decades, most of which are focused on the impact of single spatial element on the microclimate. The research topic on the correlation between wind environment and buildings first appeared during the International Conference on Building Structures and Wind Effects (Baines, 1963). After that, scientists have carried out many detailed research work around this topic. The results of (Melbourne and Joubert, 1971)'s research proved the positive correlation between building height and wind speed. After comparing the measured and simulated data, (T. Stathopoulos and Wu, 1995) indicated that the wind field around buildings can be accurately predicted. After simulating and analyzing the wind environment of more than 20 high-density residential areas, researchers from Hong Kong found a linear relationship between spatial indicator and wind velocity (Wong et al., 2010). (Tsang et al., 2012) studied the impact of spatial characteristics of building group on the wind field. The results showed that the increases of building width will reduce the efficiency of natural ventilation of pedestrian heigh. Researchers from Malaysia determined the physical indicators that affect the wind environment by simulating the airflow around the building(Abd Razak et al., 2013). Their study revealed that the frontal area ratio is the most important index affecting the wind environment at pedestrian height. (Zheng et al., 2016) simulated the wind field on the platform of mega tall building by using a combination of computational fluid dynamics (CFD) and wind tunnel experiment. (Adamek et al., 2017) pointed out that reasonable decision-making in the initial stage of urban design and planning can effectively reduce the potential safety hazards to pedestrians caused by poor wind environment. (Tse et al., 2017) studied the relationship between twisted air flows and wind field between high-rise buildings. They proved that the impact of the passage width on wind environment is more significant than that of building height in twisted wind flows. (Li et al., 2017) studied wind-induced torques on buildings. (Dai et al., 2018) evaluated the physical indicators affecting the pollutant dispersion in building arrays through CFD simulations. (Msa and Yt, 2021) proposed a novel wind environment optimization framework, in which they emphasized that the local wind environment should be considered in architectural design. (Yda et al., 2021) studied ventilation and interunit dispersion under the real urban environment, they conducted scaled outdoor experiments in street canyons in two weather periods. Another group of scholars from China studied the characteristics of roof wind field through field measurement, and summarized the variation law of roof wind field parameters (Zou et al., 2021). A study conducted by the Chinese University of Hong Kong has found that the use of Geographic Information System (GIS) data of open spaces leads to more accurate wind predictions than using road data. This research highlights the importance of utilizing accurate and comprehensive data in predicting wind patterns (Y. He et al., 2022). Through the integration of multiple models, scholars have discovered that the order of ventilation potential in various types of urban areas is as follows: road space, green space, and river space (W. Wang et al., 2022). There are also several interdisciplinary research studies related to the wind environment. For instance, a team from Tsinghua University has developed a comprehensive framework for modeling wind environment and pollutant dispersion in building clusters (Leng et al., 2022).

Although the research on this subject has been carried out for many years, there are still some problems that need to be further explored. On the one hand, the quantitative analysis of the association between wind environment and spatial indicators is insufficient. On the other hand, most of the analyzed urban spatial indicators are basic spatial indicators such as building width and building height. Nevertheless, these indicators are not enough for practitioners related to urban design. Therefore, from the perspective of designers, we comprehensively considered building footprint ratio (BFR)%, mean building height (MBH) (m) and Stagger ratio of building height (SRBH) and enclosure degree (ED) that can effectively represent urban form. And carried out the quantitative relationship analysis between these four indicators and wind environment in this study.

1.3. Research objective

The purpose of this study is to find out spatial indicators associated with wind environment, and then quantify the impact of these indicators on the wind environment of commercial streets.

The first part included the introduction of the research area and the methods used for this research. The second part was about the theoretical model and simulation process of wind environment. On one hand, the association between the spatial form of the commercial block and the wind velocity inside and around it was analyzed through correlation analysis, based on which the urban space optimization strategies were put forward. On the other hand, the effectiveness of these strategies was verified by combining field measurement with simulation, using Tang West Market and three other cases. A detailed analysis of the research results was presented in the last part.

2. Material and methods

2.1. Research area

Xi'an (Fig. 1), also known as Chang'an, is one of the four ancient capitals in the world. It is the biggest industrial and the educational center in the Northwest of China. Xi'an has four distinct seasons, among which the average temperature in summer is 27.2 °C. The average wind speed in summer is about 1.6 m/s, and the dominant wind direction is northeast wind. The main microclimate problems existing in Xi'an are weak ventilation, severe air pollution and severe heat island effect.

According to the effective wind energy density and occurrence frequency, the Chinese Academy of Meteorological Sciences divides China into four levels of wind energy regions. Among them, Xi'an belongs to an area lacking wind energy. It is difficult to form a large-scale air circulation here because of the surrounding mountains. As a typical weak wind city, low wind speed of Xi'an makes it difficult to dissipate the heat near the ground, which further aggravates the heat island effect. To optimize the wind environment of Xi'an, we took it as a research area to quantitatively analyze the relationship between wind environment and four spatial form indicators.

We conducted a spatial analysis and statistics of all commercial blocks in Xi'an and selected 44 commercial blocks that meet the research requirements. Then they were divided into four categories according to typology in the field of architectural design: centralized high-rise commercial blocks, centralized large-scale commercial blocks, mixed multi-storey commercial blocks and decentralized low-rise commercial blocks. The specific grouping and distribution are shown in Fig. 1.

To discuss the correlation between different spatial models and wind environment more comprehensively, we selected cases from

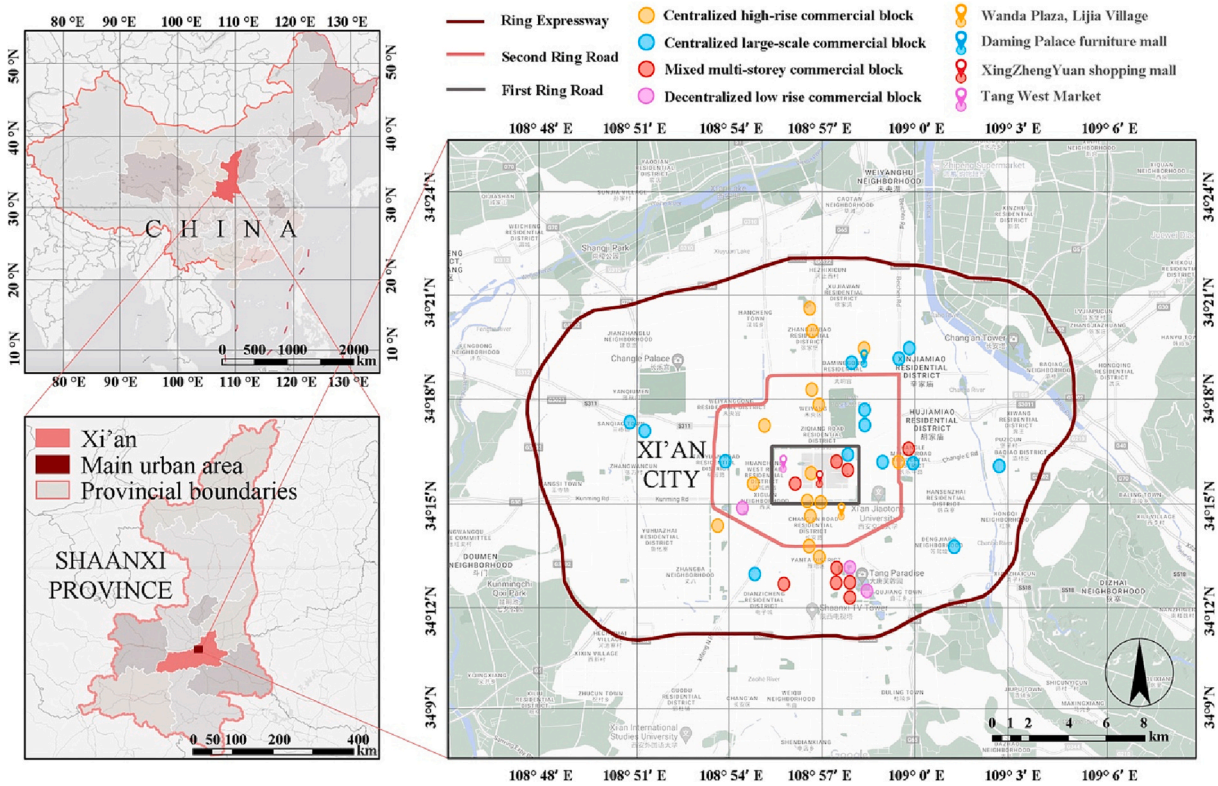

Fig. 1. The location of Xi'an.

each group that can represent the spatial characteristics of their group for further research, namely: Wanda Plaza in Lijia village, Daming Palace furniture market, XingZhengYuan shopping mall and Tang West Market (Fig. 4). Daming Palace Furniture market is a low-rise large-scale single building, and its architectural form is relatively simple. As a multi-storey building group, XingZhengYuan shopping mall is a mixture of old and new buildings, including three single buildings and many dense residential buildings. Tang West Market consists of eight single buildings and a square. The layout of Wanda Plaza is very compact, including several high-rise residential buildings, with a large shopping center at the bottom. These four different commercial blocks have the characteristics of spatial pattern and commercial activities that all commercial blocks in Xi'an have. And there is a stable flow of customers and commercial activities, so we chose these four blocks as the main research objects.

2.2. Field measurement of wind environment

2.2.1. Measurement time and instrument

According to the historical meteorological data of Xi'an Meteorological Bureau, the dominant wind direction in summer of Xi'an city is the wind of northeast wind (NE), northeast by north (NEN) and the wind of northeast by east (NEE). We conducted field measurements from April 23 to May 2nd, 2021, every day from 10 a.m. to 4 p.m. Table 1 shows the wind environment data of urban meteorological stations on the measuring days.

We used KX hand-held anemometer (Fig. 2) produced by Beijing Shunxiang Kaixin technology company to measure wind speed and direction. Table 2 presents the specific parameters of the measuring instrument.

2.2.2. Distribution of measuring points

After comparing the physical characteristics of dozens of commercial blocks in Xi'an City, we selected the commercial block of Tang West Market for field measurement. This is because this commercial block has both large-scale commercial buildings and small-scale commercial pedestrian streets. The spatial characteristics of most other commercial blocks can be found here.

The transpiration of plants has a noticeable effect on the urban microclimate (Bois et al., 2021), including wind and thermal environments, particularly in the afternoon. To minimize the impact of plant transpiration on the study results, all measuring points were placed in open sites without any plants. We arranged eight measuring points in the east entrance square and a north-south pedestrian street according to the spatial characteristics of Tang West Market. Fig. 3 shows the specific location of the measuring points. The bases for selecting measuring points include spatial characteristics and wind direction factors. Measuring point 1 is located in the upwind direction of the block, at the air inlet of the square, measuring point 2 is located in the center of the square, measuring point 3 is located in the downwind direction of the square, and measuring point 4 is located at the air outlet of the square. Measuring point 5 is located in the upwind direction of the pedestrian street on the west side, which is the air inlet of the pedestrian street. Measuring points 6 and 7 are located in the middle of the pedestrian street. Measuring point 8 is located in the downwind direction of the street, which is the air outlet of the pedestrian street. The spatial characteristics and wind direction of the positions of the eight measuring points can represent most of the situations in the measured area.

2.2.3. Analysis of measurement results

After calculating the wind environment data obtained from the field measurement, we selected the measurement section where the upwind is the NE, NEN and NEE wind (the dominant wind direction in summer of Xi'an) for five consecutive minutes. And then calculated the average wind speed of each measuring point, which is listed in Table 3. As exhibited in Table 3, the average wind speed of each measuring point does not exceed 1 m/s, except for measuring point 1. The average speed of winds of the entrance square is 0.67 m/s. The data of measuring points 2 and 4 are lower than that of measuring points 1 and 3. The average wind speed of the pedestrian street is 0.5 m/s. Among them, measuring point 6 is in a calm state most of the time. (See Table 4.)

Table 1
Wind environment data of Xi'an meteorological station from April 23 to May 2, 2021.

Time	Average Wind Speed (m/s)	Main Wind Direction
2021/4/23	3	NNE
2021/4/24	2.7	NE
2021/4/25	3.1	NNE
2021/4/26	3.3	NE
2021/4/27	2.5	NE
2021/4/28	2.2	SW
2021/4/29	2.7	NNE
2021/4/30	1.6	N
2021/5/1	3	NE
2021/5/2	2.9	NE
Average	2.7	–

Fig. 2. KX hand-held anemometer.

Table 2
Parameters of the measuring instrument.

Parameters	Instrument	Accuracy	Measuring range	Acquisition frequency	Recording mode
Wind speed	KX	±0.3 m/s	0-30 m/s	1 min	Automatic
Wind direction	KX	±1/2azimuth	0–360 angle	Instantaneous	Manual

2.3. The numerical simulation

2.3.1. Simulation software

The numerical simulation is a widely used method for wind environment prediction based on the CFD. In this study, the CFD simulation software we selected is STREAM, which is a general-purpose fluid simulation software developed by Cradle, Japan.

The use of streaming software includes three steps. Firstly, the pre-processing module is mainly used to generate and set the simulated model. To be specific, we need to import the 3D model into the pre-processing module, set various simulated condition parameters and then divide the calculation grid. Secondly, the solving module is used for simulated calculation, that is, to calculate the model generated by the pre-processing module and output the calculation result. Finally, the post-processing module helps researchers complete the final visualization of calculation results of the solving module.

There are many basic equations involved in the numerical simulation calculation of STREAM software. We describe the important parts of different numerical models as below. It should be noted that the flow field is assumed to be non-static and incompressible flow mode (X. Wang et al., 2023).

Mass conservation equation

$$\frac{\partial u_i}{\partial x_i} = 0 \tag{1}$$

Momentum conservation equation

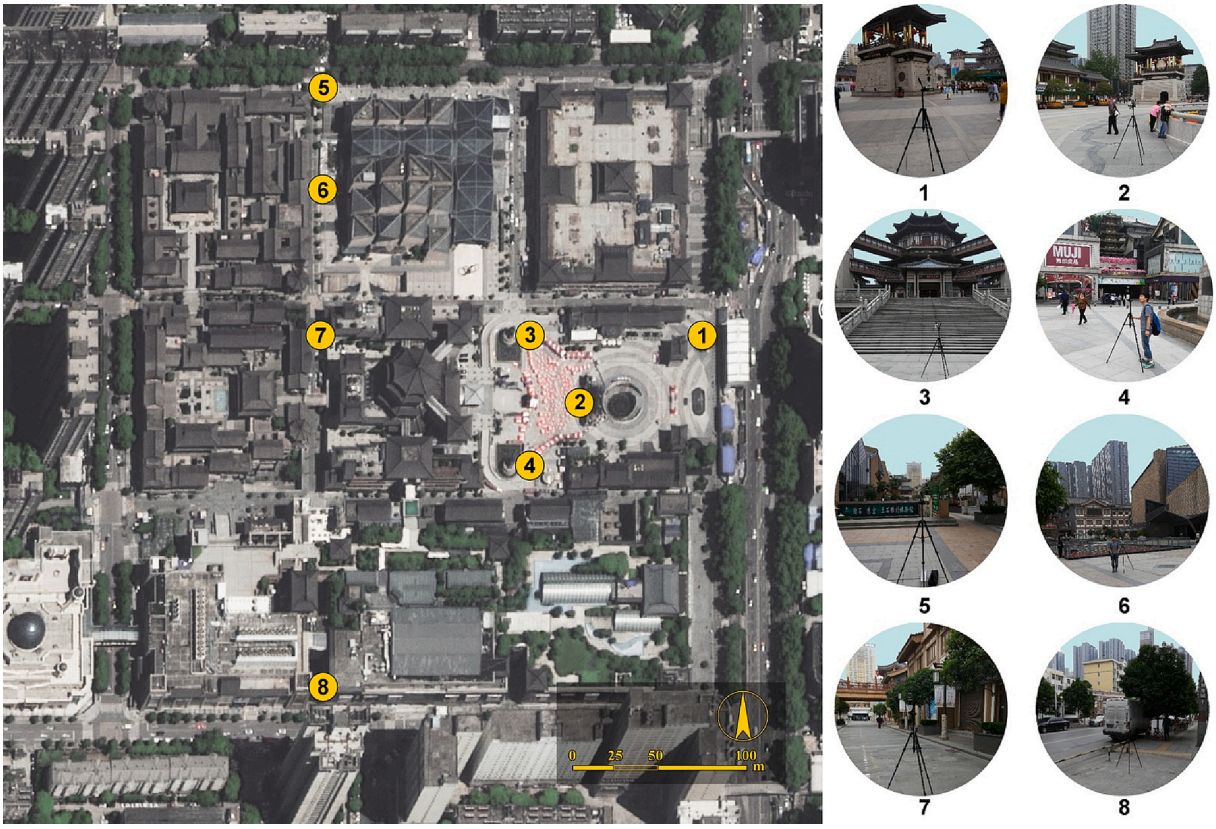

Fig. 3. Locations and surroundings of measuring points.

Table 3
Measured daily average wind speed (m/s) at 1.5 m from April 23 to May 2, 2021.

Measuring points	Entrance Square				Pedestrian Street			
	1	2	3	4	5	6	7	8
2021/4/23	2.3	0.9	0.7	0.6	0.8	0	0.3	0.8
2021/4/24	2.4	0.9	0.6	0.6	0.7	0.2	0.2	0.8
2021/4/25	2.3	1	0.8	0.7	0.7	0.1	0.4	0.9
2021/4/26	2.6	1	0.7	0.8	1	0.2	0.3	0.8
2021/4/27	2.1	1	0.5	0.5	0.8	0	0.2	0.6
2021/4/28	2.3	1	0.5	1.2	0.5	0.1	0.1	0.9
2021/4/29	2.3	0.8	0.6	0.9	0.7	0	0.4	0.5
2021/4/30	1.9	0.9	0.5	0.7	0.4	0	0.3	0.5
2021/5/1	2.1	1.1	0.6	0.8	1	0	0.4	0.7
2021/5/2	2.2	1.1	0.5	0.8	0.8	0.2	0.2	0.8
Average	2.25	0.97	0.6	0.76	0.74	0.08	0.28	0.73

$$\frac{\partial \rho u_i}{\partial t} + \frac{\partial u_j \rho u_i}{\partial x_j} = -\frac{\partial p}{\partial x_i} + \frac{\partial}{\partial x_j}\mu\frac{\partial u_i}{\partial x_j} - \rho g_i \beta (T - T_0) \tag{2}$$

Energy conservation equation

$$\frac{\partial \rho C_p T}{\partial t} + \frac{\partial u_j \rho C_p T}{\partial x_j} = \frac{\partial}{\partial x_j} K \frac{\partial T}{\partial x_j} + \dot{q} \tag{3}$$

Turbulent kinetic energy and its dissipation rate equation

$$\frac{\partial \rho k}{\partial t} + \frac{\partial u_i \rho k}{\partial x_i} = \frac{\partial}{\partial x_i}\left(\frac{u_t}{\sigma_k}\frac{\partial k}{\partial x_i}\right) + G_S + G_T - \rho\varepsilon \tag{4}$$

Table 4
The meaning of letters in the equation(Gupta and Khare, 2021; Wen et al., 2023).

Letters in equation	Meaning	Unit
C	Concentration of diffusers	[l]
C_p	Constant pressure specific heat	[J/(kg•K)]
D_m	Diffusion coefficient	[m^2/s]
d	Source term of diffusion	[l/s]
K	Thermal conductivity	[J/(m^3•s)]
k	Turbulent kinetic energy	[m^2/s^2]
P	Fluid pressure	[N/m^2]
q	Heat source	[J/(m^3•s)]
R	Gas constant	[J/(kg•K)]
T	Temperature of liquid or solid	[K]
T_0	Reference temperature of fluid	[K]
t	Time	[s]
u_i	Velocity in direction	[m/s]
VOF(n)	Volume fraction of the nth fluid	
x_i	Coordinate	[m]
β	Coefficient of thermal expansion	[l/K]
ε	Eddy dissipation rate	[m^2/s^3]
μ	Fluid viscosity	[kg/(m•s)] = [Pa•s]
ρ	Liquid density or solid density	[kg/m^3]

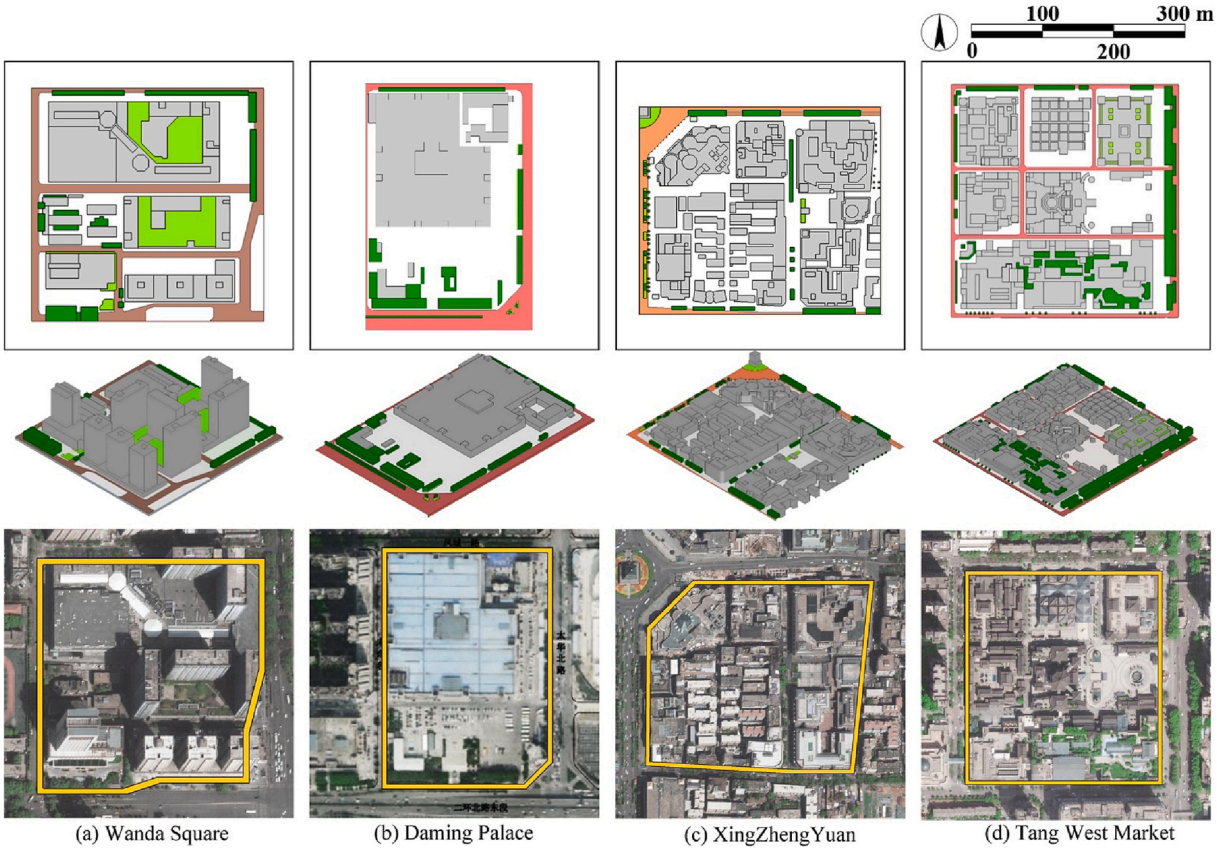

Fig. 4. Four research case models and their surrounding scenes.

$$\frac{\partial \rho\varepsilon}{\partial t}+\frac{\partial u_i\rho\varepsilon}{\partial x_i}=\frac{\partial}{\partial x_i}\left(\frac{u_t}{\sigma_\varepsilon}\frac{\partial\varepsilon}{\partial x_i}\right)+C_1\frac{\varepsilon}{k}(G_S+G_T)\left(1+C_3R_f\right)-C_2\frac{\rho\varepsilon^2}{k} \tag{5}$$

Diffusion conservation equation

$$\frac{\partial C}{\partial t}+\frac{\partial u_j C}{\partial x_j}=\frac{\partial}{\partial x_j}D_m\frac{\partial C}{\partial x_j}+\dot{d} \tag{6}$$

Fluid volume fraction conservation equation

$$\frac{\partial VOF_n}{\partial t}+u_j\frac{\partial VOF_n}{\partial x_j}=0\ (n=1,2) \tag{7}$$

Several scholars have conducted simulation research on the wind environment at pedestrian height (1.5 m) from various angles. Through their research in Changsha, China, the team found that plants have a quantifiable impact on the pedestrian-level wind environment (Shen et al., 2023). Additionally, other scholars have examined Shenzhen as an example, providing planning guidance for urban development improvements (Liu et al., 2022).

2.3.2. Setting of simulation parameters

We chose the RNG k-ε model to simulate the air turbulence and set up a steady flow field in the calculation domain. In addition, we set the air flow in the calculation domain as incompressible fluid and the basic type of boundary as external flow field, namely: Simulating the actual situation of wind blowing over the building. The boundary conditions are set to simulate the roughness around the area: surrounding medium-scale buildings (4–9 storey buildings). The boundary conditions for incoming flow are 3 m/s northeast wind at a height of 10 m (the dominant wind in Xi'an). The boundary condition for outflow is natural outflow. The boundary conditions of the building surface and ground are set to non-slip wall. Other boundary conditions are software default values. The set model is divided into 0.1 m–1 m computational grid, and then it is imported into STsolver for solution calculation. Finally, importing the calculated file into the post-processing module to view the simulation results.

2.3.3. Simulation of wind environment in four research cases

We used the modeling software sketch up to conduct three-dimensional modeling of the four cases and their surrounding buildings, which are shown in Fig. 4. The modeling data are from field measurement, Baidu satellite map and street view map.

By comparing the spatial forms of four different types of commercial blocks, we found that the building footprint ratio and enclosure degree of different types of commercial blocks has little difference. The mean building height and stagger ratio of building height of different types of commercial blocks vary greatly, among which the mean building height of centralized high-rise commercial blocks is the highest and that of decentralized low-rise commercial blocks is the lowest. In terms of the stagger ratio of building height, because the centralized high-rise commercial block is composed of high-rise buildings and bottom commercial podium, its stagger ratio of building height is significantly greater than the other three types of commercial blocks.

Then we simulated the wind environment inside and around the block according to the steps mentioned above. Fig. 5 presents the wind speed cloud diagram and wind speed vector diagram at 1.5 m height.

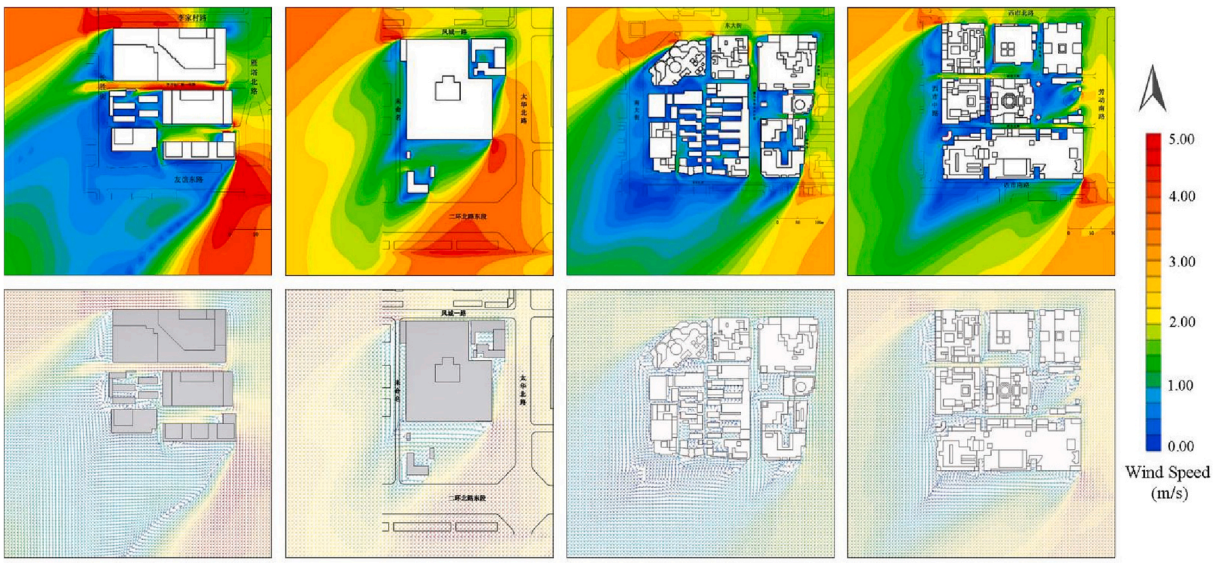

(a) Wanda Square in Lijia village (b) Daming Palace furniture market (c) XingZhengYuan shopping mall (d) Tang West Market

Fig. 5. Wind speed diagrams at 1.5 m height of the four research cases.

We mainly analyzed the wind environment simulation results of Tang West Market because it is the selected area for field measurement. As demonstrated in the Fig. 5, the wind speed in most areas of the Tang West Market is less than 1.5 m/s. Although there is a high wind speed in the eastern side urban road, it is difficult for external wind to enter the block due to the high enclosure and high building density of areas along the street. We can see from the lower part of Fig. 5 that the layout of buildings has a significant impact on the wind direction. When the external northeast wind enters the block, it changes to north wind and east wind along the outer walls of the buildings. In addition, many vortices are formed in the block due to the obstruction of buildings and the rugged street section, the most obvious of which are located at the north end of the north-south pedestrian street and the concave part of the buildings.

2.3.4. Error analysis of measurement and simulation

The simulated average wind speed and the corresponding measured data of each measured point are shown in Table 5. After linear regression analysis of the two groups of wind speed data, we found a strong linear correlation between the measured and the simulated average wind speed, which is shown in Fig. 6.

Table 5 also shows the difference between the two groups of wind speeds, from which we can see that there is an uneven difference between the measured and the simulated data of each measuring point. Among them, the difference between the two groups of wind speeds at measuring point 1 is the largest, reaching 0.95 m/s. The reason for these differences is because that the initial value of urban incoming wind set in the simulation is from Xi'an meteorological station on those 10 measuring days, which is 2.7 m/s. In fact, when the external wind enters the block, it will lose some speed because of the obstruction of surrounding buildings. Therefore, we obtained the results that the simulated data is higher than the measured data as shown in Table 5. After explaining the data error caused by the initial wind speed value, the simulation method we used can accurately describe the characteristics of wind environment of commercial blocks in Xi'an.

2.4. Urban spatial form indicators

In the past decades, scholars have found that various urban spatial form indicators are related to urban wind environment, from which we selected four indicators related to urban design and architectural design to accurately quantify their influence on wind environment, namely: BFR, MBH, SRBH and ED. The definitions or calculation methods of these spatial form indicators refer to the works of (Q. Zhang et al., 2020).

2.5. Evaluation standard of wind environment

1.5 m is the average height range of human trunk activities, and the atmosphere at this height is relatively stable and sensitive, which can better show various microclimate changes (X. Zhang et al., 2023). Therefore, the evaluation indicator of the wind environment in this paper mainly considers the average speed of winds at 1.5 m height inside and around the block. The specific calculation method is to select points equidistantly at 1.5 m from the ground in the research area to calculate the dimensionless average speed of winds where there is no construction. There are several different evaluation standard for the comfort of pedestrian wind environment (Janssen et al., 2013) (Ted Stathopoulos, 2006). In this study, we selected a commonly used one proposed by (Adamek et al., 2017).

3. Results and discussion

3.1. Establishment of theoretical model

Influenced by the urban layout of Chang'an City in Tang Dynasty (618–907 A.D), the blocks in Xi'an are mostly in square shape with the side length of about 300 m. Therefore, a 300 m × 300 m model block was set as the experimental object, and different models were established according to the changes in the selected four indicators, which are shown in Fig. 7.

BFR refers to the proportion of the total building area divided by the total land area. The model building method based on the change of BFR is as follows: In a square plot of 300 m × 300 m, the average height of the buildings is 20 m (usually a four-story commercial building), and the building density of the paved land is 100%. When using 4 vertical roads to divide it into 9 homogeneous masses, the building density is reduced to 81%. Then divide the 9 buildings into 4 small blocks of the same size, that is, when the block becomes 6 × 6 small blocks, the building density becomes 56.3%. Finally, the number of small blocks is reduced and arranged according to the pattern of 5 × 5, 4 × 4, 3 × 3, and the building density is 39.1%, 25%, and 14.1% respectively.

The modeling method by controlling the MBH is as follows: In a 300 m × 300 m square land, the buildings are arranged as shown in the second row of Fig. 7, and the buildings height are set to 10 m, 20 m, 40 m, 60 m, 80 m and 100 m, while keeping the building density unchanged. The method of establishing a model based on the change of SRBH is as follows: In a 300 m × 300 m square land, the

Table 5
Measured and simulated average speed of winds data.

Measuring points	1	2	3	4	5	6	7	8
Measured Wind Speed	2.25	0.97	0.6	0.76	0.74	0.08	0.28	0.73
Simulated Wind Speed	3.2	1.3	0.7	1.3	1.2	0.3	1.1	1.5
Wind Speed Difference	0.95	0.33	0.1	0.54	0.46	0.22	0.82	0.77

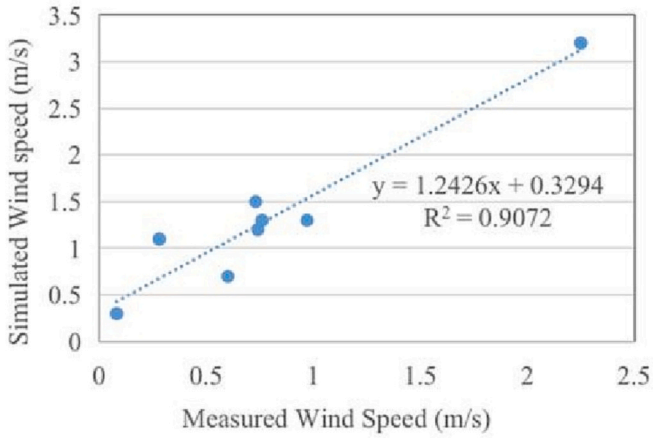

Fig. 6. Unitary regression analysis results between the measured and the simulated average wind speed.

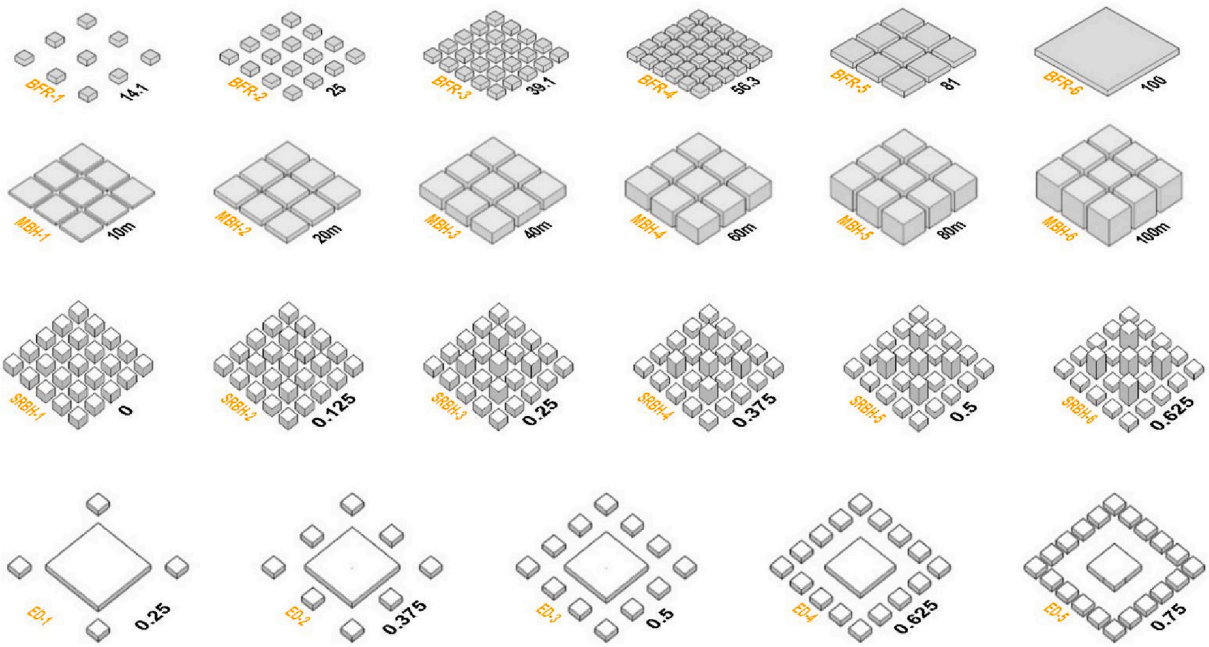

Fig. 7. The models built based on changes in BFR, MBH, SRBH and ED.

buildings are arranged as shown in the third row of Fig. 7. While keeping the building density unchanged, the mean building height is set to 40 m, and the degree of staggering is 0, 0.125, 0.25, 0.375, 0.5 and 0.625 respectively. The model building method based on the change of ED is as follows: In a 300 m × 300 m square land, the surrounding buildings are placed at equal intervals according to 2 × 2, 3 × 3, 4 × 4, 5 × 5, and 6 × 6 arrangement mode. The density of the center of the plot is gradually reduced to ensure that the overall building density remains unchanged. Their enclosure degrees are 0, 0.125, 0.25, 0.375, 0.5, and 0.625 respectively.

We imported the established models into the pre-processing module of STREAM software and set the computational domain to 1500 × 1500 × 200 m. The simulating conditions of the software were set according to the previous introduction in 2.3.2.

3.2. Association between the urban spatial form and the wind environment

3.2.1. Association between urban spatial form indicators and average speed of winds

The wind speed cloud diagrams at 1.5 m height in the block simulated by the models of changing the BFR, MBH, SRBH and ED are shown in Fig. 8. As exhibited in the diagrams of the BFR group, with the increase of building density, the external air flow entering the block will gradually decrease. As shown in Table 6, the minimum average wind speed occurs when the BFR is 56.3%. When the BFR increases from 14.1% to 56.3%, the average wind speed drops by 1.39 m/s. The average wind speed increases by 0.56 m/s as the BFR

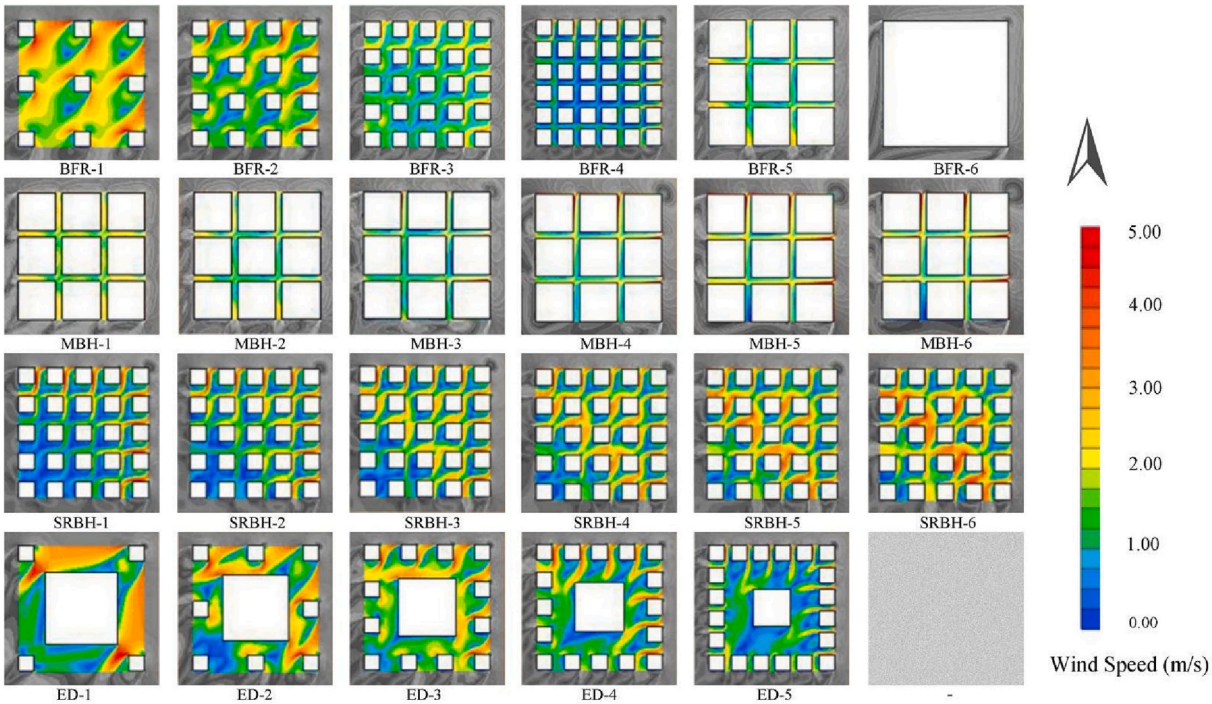

Fig. 8. The wind speed cloud diagram simulated by the model of changing the BFR, MBH, RABH and ED.

Table 6
Simulation data statistics of the models of changing the BFR, MBH, SRBH and ED.

BFR (%)	Average Wind Speed (AWS) (m/s)	MBH (m)	AWS(m/s)	SRBH	AWS(m/s)	ED	AWS (m/s)
14.1	2.08	10	1.91	0	0.63	0.25	1.74
25	1.54	20	1.25	0.125	0.86	0.375	1.70
39.1	1.02	40	1.25	0.25	1.10	0.5	1.68
56.3	0.69	60	1.52	0.375	1.33	0.625	1.31
81	1.25	80	1.71	0.5	1.53	0.75	1.14
100	/	100	1.93	0.625	1.68	/	/

rises from 56.3% to 81%.

As for the change of MBH, when this indicator rises, the wind speed of the area close to the incoming air flow direction increases, while the wind speed of the area near to the downwind direction decreases. This is because with the increase of the building height on both sides of the street, the height width ratio of the street also increases, resulting in more obvious narrow tube effect. Meanwhile, the

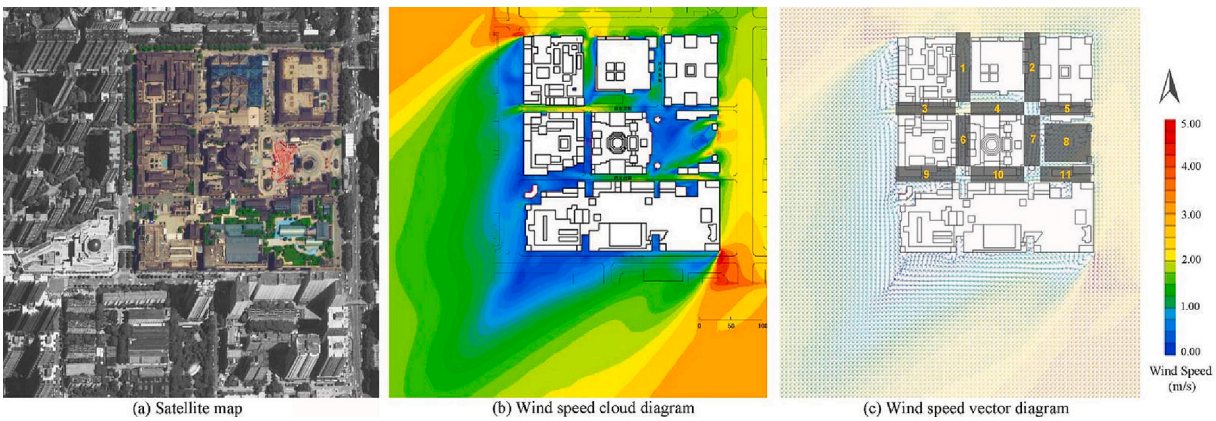

Fig. 9. The wind field diagrams and Satellite map of Tang West Market.

Fig. 10. The modification of the model of four commercial blocks.

increase of the MBH will also lead to a larger wind shadow area. Buildings in upwind direction will show greater influence on the airflow in the downwind area, which results in lower wind speeds in that area. The data listed in Table 6 show that the average wind speed inside the commercial block is minimum when the MBH is 20 to 40 m. The average wind speed decreases by 0.66 m/s when the MBH increases from 10 m to 20 m. However, when the MBH increases from 40 m to 100 m, the average wind speed increases by 0.58 m/s. The results of the correlation analysis illustrate that with the MBH increases, the average speed of winds in the block gradually decreases first and tends to be stable when the MBH approaches 20 m. When the MBH exceeds 40 m, the wind speed gradually increases.

In terms of the SRBH changing group, the average wind speed in the block increases with the increase of SRBH. This is because the air flow in the angular flow zone of the building becomes stronger with the increase of building height. Moreover, the specific expression in the spatial form of the increase in the SRBH is the increase in the unevenness of the top interface of the block, which is conducive to enhance the flow of air in the vertical direction. According to the relevant data in Table 6, the average wind speed inside the block is minimum when the SRBH is 0. When it changes from 0 to 0.625, the average wind speed rises from 0.63 m/s to 1.68 m/s. As demonstrated in the diagram of the ED changing group of models, the increase of ED of the block will reduce the average wind speed inside the block. Similar with the BFR group, as the ED increases, the amount of external air flow entering the block will gradually decrease. According to the data in Table 6, the average wind speed peaks when the enclosure degree is 0.25. When it changes from 0.25 to 0.75, the average wind speed drops from 1.74 m/s to 1.14 m/s.

3.3. Wind environment optimization strategy of commercial blocks

3.3.1. Analysis of wind environment simulation results

Since there are many common characteristics in the wind environment simulation results of the four commercial blocks, we will discuss the Tang West Market in detail, and the other simulation results are displayed in the following figures and tables. Taking the natural wind climate data of Xi'an in summer as the initial conditions, we simulated the wind environment of the Tang West Market. The wind field diagrams of pedestrian height (1.5 m) are shown in Fig. 9.

For a clearer description, we divided the outdoor space in the block into 11 areas, as shown in the Fig. 9 (b). Among them, area 8 has both the largest area and the largest wind speed difference. The maximum wind speed appears in the northwest of the small building at the entrance of the square, which is 4.28 m/s. The other 10 areas within the commercial block can be divided into two groups according to the wind speed. The first group is areas 1, 3, 4, 10 and 11 with an average wind speed of 2.79 m/s, which is within the comfortable range of outdoor wind environment (2–5 m/s). The other five areas are the second group, with an average wind speed of 0.53 m/s, and pedestrians can hardly feel the wind.

3.3.2. Spatial form adjustment strategy based on wind environment optimization

We used the theoretical models to explore the association between the wind environment and the four spatial indicators. Then obtained the corresponding value of every single spatial form indicator when the wind speed is the highest. After comparing them with the current spatial form indicators of the four research cases, we used the design method in the field of architecture to modify the spatial form in the models to improve their wind environment, which are shown in Fig. 10.

The modified standard is to make the urban spatial form indicators close to the spatial form characteristics with the highest wind speed obtained by simulation. We marked the removed parts in red on the original plan, while the area marked in blue in the modified plan indicates that the height of the building has been increased. Table 7 shows the urban physical indicators before and after the modification.

3.3.3. Verification of wind environment optimization strategy

As can be seen from the Table 7, the average wind speed at pedestrian height of Tang West Market block after spatial form optimization is 2.22 m/s, which has increased by 26.3% compared with that before optimization. The wind speed of the other three cases also increased by different ranges after spatial adjustment. Among them, although the wind speed of Daming Palace furniture market increased the least, the growth rate also reached 13.7%.

We draw the schematic diagram of point-to-point wind speed changes of main roads in Tang West Market block to compare the wind speed before and after spatial optimization in a more detailed way. As can be seen from the curves exhibited in Fig. 11, the average wind speed of road AB is 2.23 m/s, which is 0.15 m/s higher than that before spatial adjustment. Among them, the wind speed at the position with the lowest original wind speed increases by 0.29 m/s. The adjustment of block spatial shape has brought the largest growth in the wind speed to road CD, with a growth value of 0.81 m/s. The diagram of road EF illustrates that the wind speed rises steadily in the middle of the three sections of this road, although its growth value of average wind speed is limited. The wind speed at each point of the road GH fluctuates greatly, which is due to its complex spatial form. Overall, the average speed of winds of road GH is 1.58 m/s, which is 0.34 m/s higher than that before the modification.

Fig. 12 shows the wind speed cloud diagrams and wind speed vector diagrams of the other three commercial blocks before and after spatial adjustment. After spatial adjustment according to our proposed strategy, the wind environment inside and around these commercial blocks has been greatly optimized.

4. Conclusion

The purpose of this study is to determine the association between wind environment of commercial blocks and four spatial

Table 7
Comparison of indicators before and after the modification of the models of four commercial blocks.

Indicators	Wanda Plaza		Daming Palace		XingZhengYuan		Tang West Market	
	Before	After	before	After	before	After	before	After
BFR (%)	58	48	47	38	58	51	62	55
MBH (m)	31	38	19.4	15.5	21.1	24.4	13.2	12
SRBH	1.13	1.44	0.13	0.13	0.23	0.26	0.38	0.44
ED	0.79	0.69	0.59	0.46	0.85	0.82	0.81	0.75
Wind Speed (m/s)	2.39	2.88	2.77	3.15	1.52	1.97	1.79	2.22
Growth Value(m/s)	0.49		0.38		0.45		0.47	
Growth Rate(%)	16.8		13.7		29.6		26.3	

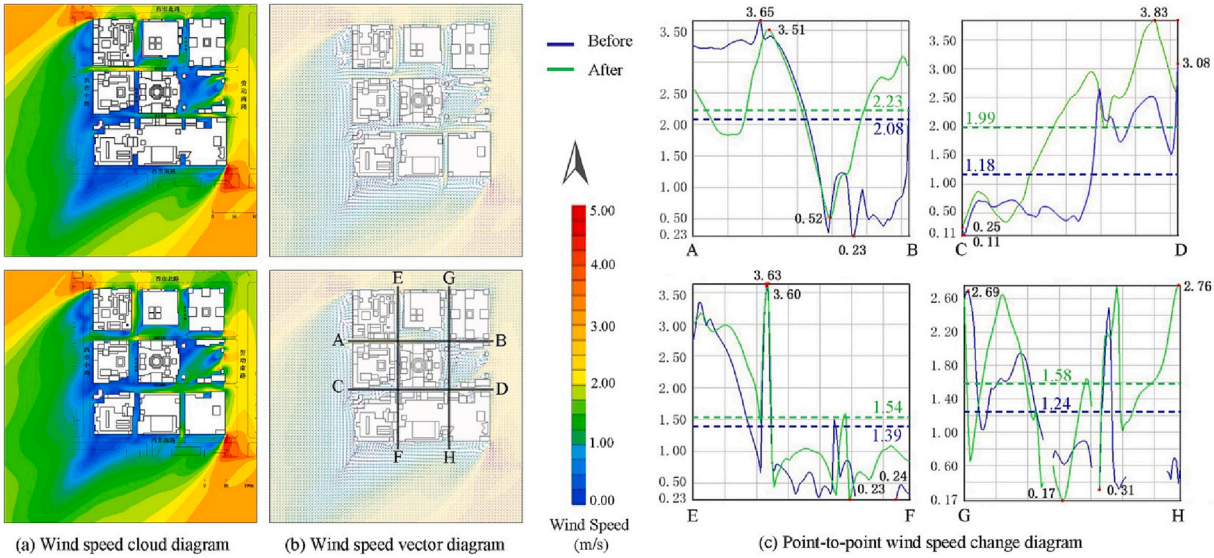

Fig. 11. Comparison of the wind speed in Tang West Market block before and after spatial optimization.

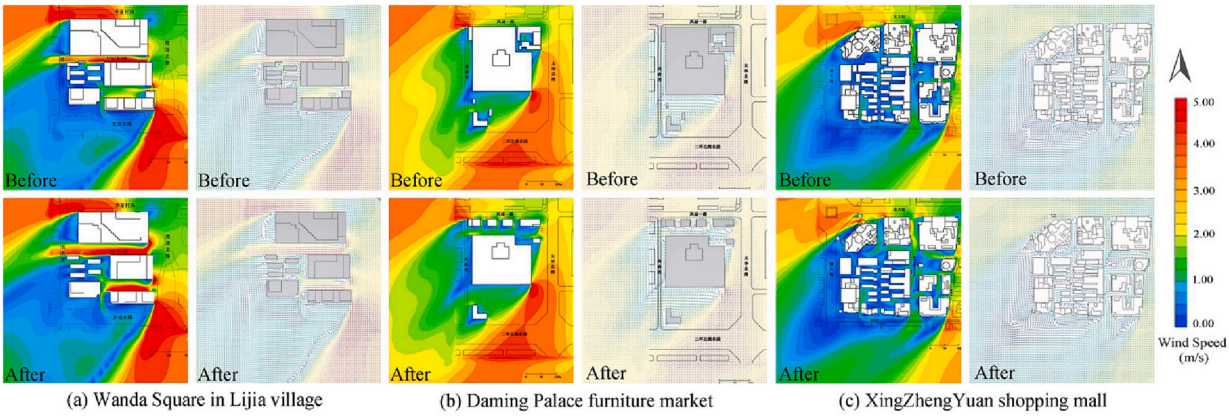

Fig. 12. Comparison of the wind speed diagrams before and after spatial optimization.

indicators related to urban design. And then draw suggestions to improve the wind environment of commercial blocks from the perspective of architectural design. We derive the following urban wind environment optimization strategies through variables controlling in software simulation.

Under the same other conditions, when the BFR reaches about 56%, the wind speed in the block is the lowest, only 0.69 m/s, which is far lower than the minimum standard of human wind environment comfort. If BFR increases or decreases based on this value, the wind speed in the block will increase. In terms of MBH, the wind speed is in a trough when the MBH of the block ranges from 20 to 40 m. In addition, the higher the MBH, the larger the wind shadow area, that is, the wind speed in downwind area will decrease with the

increase of the MBH of the upwind block. Therefore, the MBH of the commercial block should be less than 20 m. For some high-rise commercial blocks built due to land restrictions, the MBH shall be designed to exceed 40 m to ensure a comfortable wind environment in pedestrian height. Moreover, we also found quantifiable correlations between SRBH, ED and wind speed. Specifically, the wind speed of the studied block will increase with the increasing of SRBH and decrease with the rising of ED. Consequently, it is necessary to increase the SRBH of the block and reduce the ED of the block within a reasonable range to achieve better wind environment of the block and surrounding areas.

As the proposed strategies for optimizing the urban wind environment have been developed through software simulations, it is imperative to evaluate their effectiveness in actual urban designs and assess their impact on the pedestrian experience. To validate the proposed strategies, field studies combined with computer simulations can provide more accurate and reliable data. Future research should focus on the development of advanced simulation models that can account for the complex interactions between different urban elements, including trees, buildings, and roads, to provide comprehensive optimization strategies. These strategies may also incorporate innovative design solutions that enhance pedestrian comfort, reduce energy consumption, and improve air quality.

In summary, future research should build on the findings of this study to provide more effective and comprehensive strategies for optimizing the wind environment of commercial blocks and enhancing the urban pedestrian experience. These strategies are essential in creating more sustainable and livable cities.

CRediT authorship contribution statement

Qian Zhang: Writing – original draft, Writing – review & editing, Software, Methodology, Investigation, Formal analysis, Conceptualization. **Rui Dong:** Writing – original draft, Software, Methodology, Investigation. **Duo Xu:** Writing – review & editing, Funding acquisition. **Dian Zhou:** Project administration, Funding acquisition. **Alessandro Rogora:** Supervision.

Declaration of Competing Interest

The authors declare that they have no known competing financial interests or personal relationships that could have appeared to influence the work reported in this paper.

Data availability

Data will be made available on request.

Acknowledgement

This work was supported in part by the Technology Innovation Center for Land Engineering and Human Settlements, Shaanxi Land Engineering Construction Group Co…Ltd. and Xian Jiaotong University, China under grant 201912131-A5, the Chinese Scholarship Council under grant 201906280015, the Shaanxi Province Natural Science Foundation, China under grant 2022JQ-311, and the China Postdoctoral Science Foundation funded project under grant 2020 M6834975. It is a pleasure to thank an anonymous reviewer for careful reading of our manuscript and very helpful comments and suggestions.

References

Adamek, Kimberley, Vasan, Neetha, Elshaer, Ahmed, English, Elizabeth, Bitsuamlak, Girma, 2017. Pedestrian level wind assessment through city development: a study of the financial district in Toronto. Sustain. Cities Soc. 35, 178–190. https://doi.org/10.1016/j.scs.2017.06.004.

Baines, W.D., 1963. Effects of Velocity Distribution on Wind Loads and Flow Patterns on Buildings. Proc. Symp. Wind Eff. Build, p. 9.

Bois, Paul, Childers, Daniel L., Walaszek, Milena, Wanko, Adrien, 2021. Plant transpiration in constructed treatment wetland: effects on water budget and management consequences. J. Environ. Manag. 295, 113132 https://doi.org/10.1016/j.jenvman.2021.113132. https://www.sciencedirect.com/science/article/pii/S0301479721011944.

Dai, Yuwei, Mak, Cheuk Ming, Ai, Zhengtao, Hang, Jian, 2018. Evaluation of computational and physical parameters influencing CFD simulations of pollutant dispersion in building arrays. Build. Environ. 137, 90–107. https://doi.org/10.1016/j.buildenv.2018.04.005.

Dirksen, M., Ronda, R.J., Theeuwes, N.E., Pagani, G.A., 2019. Sky view factor calculations and its application in urban heat island studies. Urban Clim. 30 https://doi.org/10.1016/j.uclim.2019.100498.

Du, Sihong, Zhang, Xinkai, Jin, Xing, Zhou, Xin, Shi, Xing, 2022. A review of multi-scale modelling, assessment, and improvement methods of the urban thermal and wind environment. Build. Environ. 213, 108860 https://doi.org/10.1016/j.buildenv.2022.108860. https://www.sciencedirect.com/science/article/pii/S0360132322001068.

Elshaer, Ahmed, Gairola, Anant, Adamek, Kimberley, Bitsuamlak, Girma, 2017. Variations in wind load on tall buildings due to urban development. Sustain. Cities Soc. 34, 264–277. https://doi.org/10.1016/j.scs.2017.06.008.

Georgakis, Ch., Santamouris, M., 2006. Experimental investigation of air flow and temperature distribution in deep urban canyons for natural ventilation purposes. Energy and Build. 38 (4), 367–376. https://doi.org/10.1016/j.enbuild.2005.07.009.

Golany, G.S., 1996. Urban design morphology and thermal performance. Atmos. Environ. 30 (3), 455–465.

Gupta, Durva, Khare, Vaibhav Rai, 2021. Natural ventilation design: predicted and measured performance of a hostel building in composite climate of India. Energy and Built Environ. 2 (1), 82–93. https://doi.org/10.1016/j.enbenv.2020.06.003. https://www.sciencedirect.com/science/article/pii/S266612332030057X.

Hallegatte, Stéphane, Corfee-Morlot, Jan, 2010. Understanding climate change impacts, vulnerability and adaptation at city scale: an introduction. Clim. Chang. 104 (1), 1–12. https://doi.org/10.1007/s10584-010-9981-8.

He, Bao-Jie, Yang, Li, Ye, Miao, 2014. Strategies for creating good wind environment around Chinese residences. Sustain. Cities Soc. 10, 174–183. https://doi.org/10.1016/j.scs.2013.08.003.

He, Yueyang, Liu, Zhixin, Ng, Edward, 2022. Parametrization of irregularity of urban morphologies for designing better pedestrian wind environment in high-density cities – a wind tunnel study. Build. Environ. 226, 109692 https://doi.org/10.1016/j.buildenv.2022.109692. https://www.sciencedirect.com/science/article/pii/S0360132322009222.

Janssen, W.D., Blocken, B., van Hooff, T., 2013. Pedestrian wind comfort around buildings: comparison of wind comfort criteria based on whole-flow field data for a complex case study. Build. Environ. 59, 547–562. https://doi.org/10.1016/j.buildenv.2012.10.012.

Kastner-Klein, P., Berkowicz, R., Britter, R., 2004. The influence of street architecture on flow and dispersion in street canyons. Meteorog. Atmos. Phys. 87, 1–3. https://doi.org/10.1007/s00703-003-0065-4.

Leng, Shuo, Li, Sun-Wei, Zhen-Zhong, Hu, Hao-Yang, Wu, Li, Bin-Bin, 2022. Development of a micro-in-meso-scale framework for simulating pollutant dispersion and wind environment in building groups. J. Clean. Prod. 364, 132661 https://doi.org/10.1016/j.jclepro.2022.132661. https://www.sciencedirect.com/science/article/pii/S0959652622022600.

Li, Yi, Li, Q.S., Chen, Fubin, 2017. Wind tunnel study of wind-induced torques on L-shaped tall buildings. J. Wind Eng. Ind. Aerodyn. 167, 41–50. https://doi.org/10.1016/j.jweia.2017.04.013.

Liu, Xiaoqian, Huang, Bo, Li, Rongrong, Zhang, Junhua, Gou, Qiang, Zhou, Tao, Huang, Zhihui, 2022. Wind environment assessment and planning of urban natural ventilation corridors using GIS: Shenzhen as a case study. Urban Clim. 42, 101091 https://doi.org/10.1016/j.uclim.2022.101091. https://www.sciencedirect.com/science/article/pii/S2212095522000098.

Melbourne, W., Joubert, P., 1971. Problems of Wind Flow at the Base of Tall Buildings.

Msa, B., Yt, B., 2021. Multi-fidelity shape optimization methodology for pedestrian-level wind environment. Build. Environ. 204 https://doi.org/10.1016/j.buildenv.2021.108076.

Oke, T.R., 1988. Street design and urban canopy layer climate. Energy and Build. 11 (1–3), 103–113. https://doi.org/10.1016/0378-7788(88)90026-6.

Palusci, Olga, Monti, Paolo, Cecere, Carlo, Montazeri, Hamid, Blocken, Bert, 2022. Impact of morphological parameters on urban ventilation in compact cities: the case of the Tuscolano-Don Bosco district in Rome. Sci. Total Environ. 807, 150490 https://doi.org/10.1016/j.scitotenv.2021.150490. https://www.sciencedirect.com/science/article/pii/S0048969721055674.

Razak, Abd, Azli, Aya Hagishima, Ikegaya, Naoki, Tanimoto, Jun, 2013. Analysis of airflow over building arrays for assessment of urban wind environment. Build. Environ. 59, 56–65. https://doi.org/10.1016/j.buildenv.2012.08.007.

Shashua-Bar, Limor, Hoffman, Milo E., 2004. Quantitative evaluation of passive cooling of the UCL microclimate in hot regions in summer, case study: urban streets and courtyards with trees. Build. Environ. 39 (9), 1087–1099. https://doi.org/10.1016/j.buildenv.2003.11.007.

Shen, Lian, Han, Yan, Lihua, Mi, Lei, Xu, Guoji, Xu, Cai, C.S., 2023. Assessment of the influences of post-construction facilities on pedestrian-level wind environment: an experimental study in Changsha, China. Urban Clim. 47, 101366 https://doi.org/10.1016/j.uclim.2022.101366. https://www.sciencedirect.com/science/article/pii/S221209552200284X.

Stathopoulos, Ted, 2006. Pedestrian level winds and outdoor human comfort. J. Wind Eng. Ind. Aerodyn. 94 (11), 769–780. https://doi.org/10.1016/j.jweia.2006.06.011.

Stathopoulos, T., Wu, H., 1995. Generic models for pedestrian-level winds in built-up regions. J. Wind Eng. Ind. Aerodyn. 54 (2), 515–525.

Tsang, C.W., Kwok, K.C.S., Hitchcock, P.A., 2012. Wind tunnel study of pedestrian level wind environment around tall buildings: effects of building dimensions, separation and podium. Build. Environ. 49, 167–181. https://doi.org/10.1016/j.buildenv.2011.08.014.

Tse, K.T., Weerasuriya, A.U., Zhang, Xuelin, Li, S.W., Kwok, K.C.S., 2017. Effects of twisted wind flows on wind conditions in passages between buildings. J. Wind Eng. Ind. Aerodyn. 167, 87–100. https://doi.org/10.1016/j.jweia.2017.04.011.

Wang, Weiwu, Chen, Huan, Wang, Lizhong, Wang, Shan, 2022. Integrating multiple models into computational fluid dynamics for fine three-dimensional simulation of urban waterfront wind environments: a case study in Hangzhou, China. Sustain. Cities Soc. 85, 104088 https://doi.org/10.1016/j.scs.2022.104088. https://www.sciencedirect.com/science/article/pii/S221067072200405X.

Wang, Xiaoyu, Gong, Liang, Li, Yang, Yao, Jun, 2023. Developments and applications of the CFD-DEM method in particle–fluid numerical simulation in petroleum engineering: a review. Appl. Therm. Eng. 222, 119865 https://doi.org/10.1016/j.applthermaleng.2022.119865. https://www.sciencedirect.com/science/article/pii/S1359431122017951.

Wen, Yueming, Lau, Siu-Kit, Leng, Jiawei, Zhou, Kai, Cao, Shi-Jie, 2023. Passive ventilation for sustainable underground environments from traditional underground buildings and modern multiscale spaces. Tunn. Undergr. Space Technol. 134, 105002 https://doi.org/10.1016/j.tust.2023.105002. https://www.sciencedirect.com/science/article/pii/S0886779823000226.

Wong, Man Sing, Nichol, Janet E., Pui Hang To, Wang, Jingzhi, 2010. A simple method for designation of urban ventilation corridors and its application to urban heat island analysis. Build. Environ. 45 (8), 1880–1889. https://doi.org/10.1016/j.buildenv.2010.02.019.

Yang, Yujun, Zhou, Dian, Gao, Weijun, Zhang, Zihan, Chen, Wei, Peng, Wangchongyu, 2018. Simulation on the impacts of the street tree pattern on built summer thermal comfort in cold region of China. Sustain. Cities Soc. 37, 563–580. https://doi.org/10.1016/j.scs.2017.09.033.

Yda, B., Cmm, B., Jian, Hcd, Fz, A., Hong, Lcd, 2021. Scaled Outdoor Experimental Analysis of Ventilation and Interunit Dispersion with Wind and Buoyancy Effects in Street Canyons. https://doi.org/10.1016/j.enbuild.2021.111688.

Zhang, Aishe, Gao, Cuilan, Zhang, Ling, 2005. Numerical simulation of the wind field around different building arrangements. J. Wind Eng. Ind. Aerodyn. 93 (12), 891–904. https://doi.org/10.1016/j.jweia.2005.09.001.

Zhang, Qian, Duo, Xu, Zhou, Dian, Yang, Yujun, Rogora, Alessandro, 2020. Associations between urban thermal environment and physical indicators based on meteorological data in Foshan City. Sustain. Cities Soc. 60 https://doi.org/10.1016/j.scs.2020.102288.

Zhang, Xiaotong, Gao, Yafeng, Tao, Qiuhua, Min, Yunran, Fan, Juntao, 2023. Improving the pedestrian-level wind comfort by lift-up factors of panel residence complex: field-measurement and CFD simulation. Build. Environ. 229, 109947 https://doi.org/10.1016/j.buildenv.2022.109947. https://www.sciencedirect.com/science/article/pii/S0360132322011775.

Zheng, Chaorong, Li, Yinsong, Yue, Wu., 2016. Pedestrian-level wind environment on outdoor platforms of a thousand-meter-scale megatall building: sub-configuration experiment and wind comfort assessment. Build. Environ. 106, 313–326. https://doi.org/10.1016/j.buildenv.2016.07.004.

Zou, Q., Li, Z., Zeng, X., Wang, C., Zou, F., 2021. The analysis of characteristics of wind field on roof based on field measurement. Energy and Build. 240 (2), 110877 https://doi.org/10.1016/j.enbuild.2021.110877.